Article

Antibody-Catalyzed Oxy-Cope Rearrangement: Mechanism and Origins of Catalysis and Stereoselectivity from DFT Quantum Mechanics and Flexible Docking

Kersey A. Black, Andrew G. Leach, M. Yashar S. Kalani, and K. N. Houk

J. Am. Chem. Soc., **2004**, 126 (31), 9695-9708• DOI: 10.1021/ja048604g • Publication Date (Web): 10 July 2004

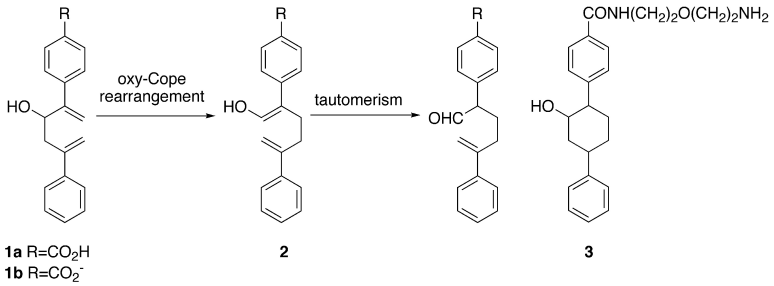

More About This Article

Additional resources and features associated with this article are available within the HTML version:

- Supporting Information
- Links to the 1 articles that cite this article, as of the time of this article download
- Access to high resolution figures
- Links to articles and content related to this article
- Copyright permission to reproduce figures and/or text from this article

View the Full Text HTML

J|A|C|S
ARTICLES
Published on Web 07/10/2004

Antibody-Catalyzed Oxy-Cope Rearrangement: Mechanism and Origins of Catalysis and Stereoselectivity from DFT Quantum Mechanics and Flexible Docking

Kersey A. Black,[‡] Andrew G. Leach,[†] M. Yashar S. Kalani,[†] and K. N. Houk*,[†]

Contribution from the Department of Chemistry and Biochemistry, University of California, Los Angeles, California 90095-1569, and Joint Science Department, Claremont Colleges, Claremont, California 91711-5916

Received March 10, 2004; E-mail: houk@chem.ucla.edu

Abstract: Density functional theory using B3LYP and flexible ligand docking methods were used to investigate the complete potential surface for the uncatalyzed and the AZ28 antibody-catalyzed oxy-Cope reaction of 2,5-diaryl-1,5-hexadien-3-ol derivatives. The reaction mechanism is stepwise, involving a cyclohexane diyl intermediate. Theoretical deuterium isotope effects match well with those from experiment. Gas-phase transition structures show mixed preferences for the axial vs equatorial hydroxyl group, while solvation favors the axial isomer. Specific phenyl group conformations are shown to be critical to transition-state stabilization (by up to 15 kcal/mol), and the effective conformation is not that found in the hapten used to generate the germline and affinity-matured AZ28 catalytic antibodies. Docking studies support greater transition-state binding than reactant binding. Docking studies also predict the *S* stereoselectivity of mature AZ28 and suggest that binding modes quite different from those of the hapten might play a role in catalysis, with specific focus on ligand hydrogen bonding to Asp^{H101}.

Introduction

Critical to most models explaining the extraordinary efficiency by which enzymes accelerate chemical reactions is the specific binding of the transition structure of the reaction. Coupling this understanding with the ability of the immune system to generate proteins which selectively bind small organic structures has provided a foundation for the field of catalytic antibodies. By generating an antibody to a stable transition-state mimic (hapten), a protein may be created that can bind the transition state more tightly than the substrate or products and thus accelerate their interconversion. In the intervening 17 years since the first application of this insight,[1] the development of monoclonal antibody technology has supported the production of antibodies as catalysts[2] for both known enzymatic reactions[3] and nonbiological transformations,[4] including synthetic and medicinal applications.

Beyond the practical potential of developing new catalysts, this methodology also provides a set of structure/function data which is unique in at least two respects. The first is the possibility to study directly the protein−transition state analogue (hapten) complex through X-ray crystallography. Second, hapten binding affinity and catalytic efficiency can be examined as a function of somatic mutation of residues in the active site as the germline structure evolves to the affinity matured antibody.[5] In total, this very rich set of structure/function data provides an unusual opportunity to study fundamentals of proteinic catalysis, as well as providing for more effective hapten design and ultimately engineering of protein catalysts.[6]

In 1994, Schultz and co-workers reported antibody catalysts that accelerate the oxy-Cope rearrangement of allylic alcohol **1** to enol **2** by factors of 10^3-10^5 (k_{cat}/k_{uncat}).[7a,b] The catalytic antibodies were raised to hapten **3** (Figure 1), which mimics the highly ordered chairlike geometry anticipated for the transition state in this 3,3-sigmatropic rearrangement. Since that time, the mechanism of catalysis by the best of these antibodies,

[†] University of California, Los Angeles.
[‡] Claremont Colleges.

(1) (a) Tramontano, A.; Janda, K. D.; Lerner, R. A. *Science* **1986**, *234*, 1566−1570. (b) Pollack, S. J.; Jacobs, J. W.; Schultz, P. G. *Science* **1986**, *234*, 1570−1573.

(2) Reviews: (a) Schultz, P. G.; Lerner, R. A. *Acc. Chem. Res.* **1993**, *26*, 391−395. (b) Schultz, P. B. *Angew. Chem., Int. Ed. Engl.* **1989**, *28*, 1283−1295. (c) Schultz, P. G.; Lerner, R. A. *Acc. Chem. Res.* **1993**, *26*, 391−395. (d) Schultz, P. G.; Lerner, R. A. *Science* **1995**, *269*, 1835−1842. (e) Hilvert, D. *Annu. Rev. Biochem.* **2000**, *69*, 751−793. (f) Hilvert, D.; MacBeath, G.; Shin, J. A. *Bioorg. Chem.: Pept. Proteins* **1998**, 335−366; 502−505. (g) Hilvert, D. *Curr. Opin. Struct. Biol.* **1994**, *4*, 612−617. (h) Hilvert, D. Stereoselective reactions with catalytic antibodies. *Top. Stereochem.* **1999**, *22*, 83−135. (i) Wentworth, P.; Janda, K. D. *Cell Biochem. Biophys.* **2001**, *35*, 63−86. (j) Tellier, C. *Transfus. Clin. Biol.* **2002**, *9*, 1−8. (k) Barbany, M.; Gutierrez-de-Teran, H.; Sanz, F.; Villa-Freixa, J.; Warshel, A. *ChemBioChem* **2003** *4*, 277−285. (l) Tanaka, F. *Chem. Rev.* **2002**, *102*, 4885−4906.

(3) (a) Shreder, K. *Methods* **2000**, *20*, 372−379. (b) Raso, V.; Stollar, B. D. *Biochemistry* **1975**, *14*, 591−597. (c) Lerner, R. A.; Janda, K. D. *EXS* **1995**, *73*, 121−128. (d) Hasserodt, J.; Janda, K. D.; Lerner, R. A. *J. Am. Chem. Soc.* **2000**, *122*, 40−45. (e) Bjornestedt, R.; Zhong, G.; Lerner, R. A.; Barbas, C. F., III. *J. Am. Chem. Soc.* **1996**, *118*, 11720−11724. (f) Janda, K. D.; Schloder, D.; Bankovic, S. J.; Lerner, R. A. *Science* **1988**, *241*, 437−440. (g) Haynes M. R.; Stura E. A.; Hilvert D.; Wilson I. A. *Science* **1994**, *263*, 646−652. (h) Mitsuda, Y.; Hifumi, E.; Tsuruhata, K.; Fujinami, H.; Yamamoto, N.; Uda, T. *Biotechnol. Bioeng.* **2004**, *86*, 217−225. (i) Aggarwal, R.; Benedetti, F.; Berti, F.; Buchini, S.; Colombatti, A.; Dinon, F.; Galasso, V.; Norbedo, S. *Chem. Eur. J.* **2003**, *9*, 3132−3142. (j) Saveliev, A. N.; Ivanen, D. R.; Kulminskaya, A. A.; Ershova, N. A.; Kanyshkova, T. G.; Buneva, V. N.; Mogelnitskii, A. S.; Doronin, B. M.; Favorova, O. O.; Nevinsky, G. A.; Neustroev, K. N. *Immunol. Lett.* **2003**, *86*, 291−297.

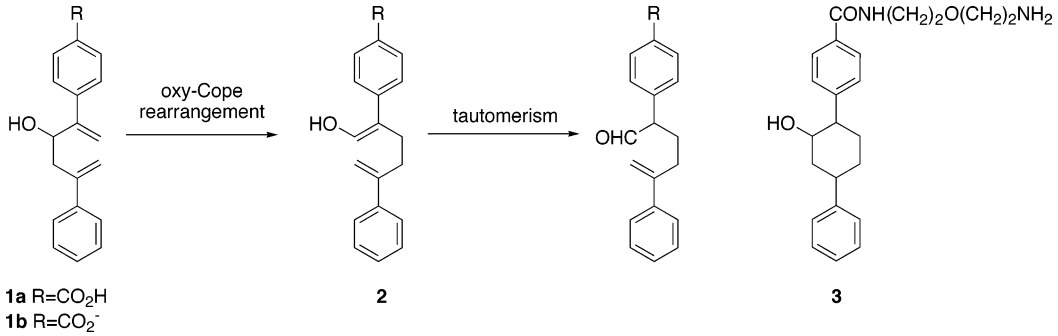

Figure 1. Oxy-Cope rearrangement of **1** to **2**, and hapten (**3**) for antibody generation.

AZ28, has been probed by experimental investigations[7] and one theoretical study.[8]

In this paper, we provide a density functional theory (DFT) analysis of the oxy-Cope reaction of **1** and the results of using automated docking methods to explore the binding of the hapten, starting materials, and possible transition structures in both the affinity-matured antibody (AZ28m) and its germline precursor (AZ28g).

Background

Kinetic studies, NMR measurements, and X-ray crystallographic data for both germline and mature forms of AZ28 have revealed remarkable details about how these antibodies bind the hapten and catalyze this simple rearrangement.[7]

Kinetic experiments have shown that mature antibody AZ28m lowers $\Delta H^{\ddagger}$ from 27.4 kcal/mol for the uncatalyzed reaction to 15.4 ± 2.4 kcal/mol for the catalyzed process.[7c] This favorable change in enthalpy offsets a very unfavorable change in $\Delta S^{\ddagger}$, which is −3 cal/(mol K) for the uncatalyzed reaction and −23 ± 8 cal/(mol K) for the antibody-catalyzed process. While

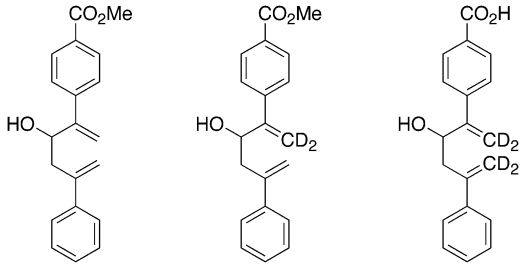

Figure 2. Three structures used to establish kinetic isotope effects on the reaction catalyzed by antibody AZ28.

hydroxyl substitution at C3 provides the only chiral center in the reactant, stereochemistry at this position has a significant impact on the rate of the antibody-catalyzed reaction. The k_{cat} for the *S* isomer is 15.1 times larger that than for the *R* isomer.[7c] Kinetic measurements have also revealed that, whereas the substrate is bound to approximately the same degree by both the mature AZ28m (K_M = 74 μM) and the germline AZ28g (K_M = 73 μM), the transition structure of the reaction is bound more tightly by the germline form ($K_{TX} = k_{uncat}K_M/k_{cat}$ = 14 nM) than the mature form (K_{TX} = 4.5 nM).[7c] Hence, one intriguing result of the kinetic work is that, even though the hapten (expected to be transition-state analogue) is bound more tightly by AZ28m (K_D = 17 nM) than by AZ28g (K_D = 670 nM), the germline form binds the actual transition state better and is a more effective catalyst.

Secondary kinetic isotope effects for the reactions corresponding to both k_{cat} and k_{cat}/K_M were measured using the analogues shown in Figure 2.[7c] Competition experiments between **4** and the dideuterated **5** (solubilized using CH_3CN cosolvent) determined that there is a secondary deuterium isotope effect of 0.72 ± 0.03 for the process corresponding to k_{cat}/K_M. Comparison of the rate of antibody-catalyzed rearrangement of tetradeuterated **6** with the rate for **1** revealed a secondary isotope effect of 0.61 ± 0.1 for the process corresponding to k_{cat}. When normalized to dideuteration, this result corresponds to a value of 0.78, which is similar to that measured for k_{cat}/K_M and indicates that the sigmatropic shift is the slowest step of the overall catalyzed process (as opposed to association, dissociation, or tautomerization).

The mechanism of the uncatalyzed oxy-Cope[9] reaction has been studied extensively, in part because of the utility of this reaction as a tool for synthesis. This 3,3-sigmatropic rearrange-

(4) (a) Janda, K. D.; Shevlin, C. G.; Lerner, R. A. *J. Am. Chem. Soc.* **1995**, *117*, 2659−2671. (b) Gouverneur, V. E.; dePascul-Teressa, B.; Beno, B.; Janda, K. D.; Lerner, R. A. *Science* **1993**, *262*, 204−214. (c) Flanagan, M. E.; Jacobsen, J. R.; Sweet, E.; Schultz, P. G. *J. Am. Chem. Soc.* **1996**, *118*, 6078−6079. (d) Yoon, S. S.; Oei, Y.; Sweet, E.; Schultz, P. G. *J. Am. Chem. Soc.* **1996**, *118*, 11686−11687. (e) Uno, T.; Ku, J.; Prudent, J. R.; Huang, A.; Schultz, P. G. *J. Am. Chem. Soc.* **1996**, *118*, 3811−3817. (f) Wagner, J.; Lerner, R. A.; Barbas, C. F., III. *Science* **1995**, *270*, 1797−1800. (g) Hoffmann, T.; Zhong, G.; List, B.; Shabat, D.; Anderson, J.; Gramatikova, S.; Lerner, R. A.; Barbas, C. F., III. *J. Am. Chem. Soc.* **1998**, *120*, 2768−2779. (h) Turner, J. M.; Larsen, N. A.; Basran, A.; Barbas, C. F., III; Bruce, N. C.; Wilson, I. A.; Lerner, R. A. *Biochemistry* **2002**, *41*, 12297−12307. (i) Gruber, K.; Zhou, B.; Houk, K. N.; Lerner, R. A.; Shevlin, C. G.; Wilson, I. A. *Biochemistry* **1999**, *38*, 7062−7074. (j) Jones, L. H.; Harwig, C. W.; Wentworth, P., Jr.; Simeonov, A.; Wentworth, A. D.; Py, S.; Ashley, J. A.; Lerner, R. A.; Janda, K. D. *J. Am. Chem. Soc.* **2001**, *123*, 3607−3608. (k) Zhong, G.; Hoffmann, T.; Lerner, R. A.; Danishefsky, S.; Barbas, C. F., III. *J. Am. Chem. Soc.* **1997**, *119*, 8131−8132. (l) Chen J.; Deng Q.; Wang R.; Houk K. N.; Hilvert D. *ChemBioChem* **2000**, *1*, 255−61. (m) Guo, J. C.; Huang, W.; Scanlan, T. S. *J. Am. Chem. Soc.* **1994**, *116*, 6062−6069. (n) Driggers, E. M.; Cho, H. S.; Liu, C. W.; Katzka, C. P.; Braisted, A. C.; Ulrich, H. D.; Wemmer, D. E.; Schultz, P. G. *J. Am. Chem. Soc.* **1998**, *120*, 1945−1958. (o) Tremblay, M. R.; Dickerson, T. J.; Janda, K. D. *Adv. Synth. Catal.* **2001**, *343*, 577−585. (p) Sapier, S.; Sinha, S. C.; Keinan, E. *Angew. Chem., Int. Ed.* **2003**, *42*, 1378−1381. (q) Pungenta, M. D.; Weiler, L.; Ziltener, H. J. *Can. J. Chem.* **2002**, *80*, 1643−1645.
(5) Example of affinity matching through maturation: Yin, J.; Mundorff, E. C.; Yang, P. L.; Wendt, K. U.; Hanway, D.; Stevens, R. C.; Schultz, P. G. *Biochemistry* **2001**, *40*, 10764−10773.
(6) (a) Schultz, P. G.; Lerner, R. A. *Science* **1995**, *269*, 1835−1842. (b) Lerner, R. A.; Benkovic, S. J.; Schultz, P. G. *Science* **1991**, *252*, 659−667.
(7) (a) Braisted, A. C.; Schultz, P. G. *J. Am. Chem. Soc.* **1994**, *116*, 6, 2211−2212. (b) Ulrich, H. D.; Mundorff, E. C.; Santarsiero, B. D.; Driggers, E. M.; Stevens, R. C.; Schultz, P. G. *Nature* **1997**, *389*, 271−275. (c) Driggers, E. M.; Cho, H. S.; Liu, C. W.; Katzka, C. P.; Braisted, A. C.; Ulrich, H. D.; Wemmer, D. E.; Schultz, P. G. *J. Am. Chem. Soc.* **1998**, *120*, 1945−1958. (d) Mundorff, E. C.; Hanson, M. A.; Varvak, A.; Ulrich, H. D.; Schultz, P. G.; Stevens, R. C. *Biochemistry* **2000**, *39*, 627−632.
(8) Asada, T.; Gouda, H.; Kollman, P. A. *J. Am. Chem. Soc.* **2002**, *124*, 12535−12542.
(9) Berson, J. A.; Jones, M., Jr. *J. Am. Chem. Soc.* **1964**, *86*, 5019−5020; 5017−5018.

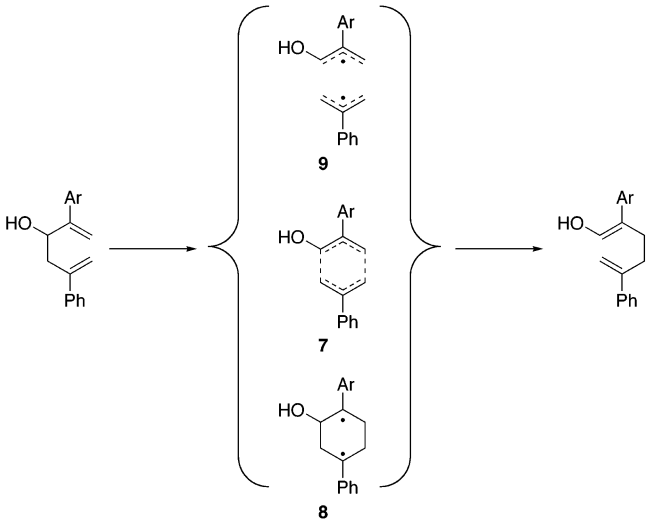

Figure 3. Three descriptions of the mechanism of the oxy-Cope rearrangement of **1**: a concerted transition state **7**, 1,4-diyl intermediate **8**, and a pair of allyl radicals **9**.

ment shares the predictable stereocontrolled outcome of the parent Cope[10] reaction and is driven to completion by the final tautomerization of the resultant enol. The utility of this thermal rearrangement was greatly enhanced by the subsequent discovery of the anionic variant, in which deprotonation of the −OH, typically by conversion to the corresponding potassium alkoxide, dramatically accelerates the process by as much as $10^{10}-10^{17}$.[11] This allows for low-temperature reaction conditions appropriate to systems involving sensitive functionality.[12]

Mechanistic understanding of this 3,3-sigmatropic rearrangement has followed on the more thoroughly studied parent process, the Cope reaction of 1,5-hexadiene.[13] For both rearrangements, three mechanisms have been postulated (Figure 3). The first is a concerted one-step process (through a transition state like **7**), as allowed for by Woodward−Hoffmann analysis. The other two mechanisms are two-step diradical processes. One begins with closure of the hexadiene to a cyclic 1,4-diyl **8**, and the other mechanism starts with homolytic cleavage to generate a pair of allyl radicals **9**. Collectively, these three pathways represent canonical descriptions between which lie a continuum of mechanistic possibilities.

The Cope rearrangement of 1,5-hexadiene has been found by experimental and theoretical studies to proceed through a concerted mechanism. Notably, secondary deuterium kinetic isotope effects computed for a concerted transition structure obtained at the B3LYP/6-31G(d) level of theory agree well with those measured experimentally.[14] The potentially competing 1,4-diyl and allyl diradical pathways are calculated to be 11 and 26 kcal/mol higher in energy, respectively.

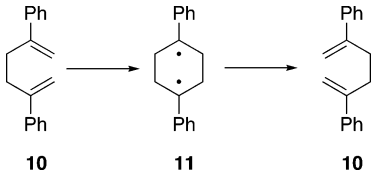

Figure 4. Mechanism of the Cope rearrangement of 2,5-diphenyl-1,5-hexadiene which passes through a diradical intermediate.

Theoretical studies of the simplest oxy-Cope rearrangement, that of 3-hydroxy-1,5-hexadiene, found a slightly asynchronous but nevertheless concerted transition state using B3LYP/6-31+G(d) methodology.[15] The preferred chairlike structure of the transition structures calculated for rearrangement of the parent system supports using cyclohexanol as a foundation in the hapten as a mimic of the transition structure. Theoretical work on the related anionic oxy-Cope variant supports a concerted one-step, though quite asynchronous, process for the rearrangement of the parent system and agree that increasing electron density on the oxy-substituent will accelerate the rearrangement.[16] Whether hydrogen-bonding and perhaps partial deprotonation of the hydroxyl in the active site can accelerate the rearrangement merits consideration. X-ray crystallographic studies of the two proteins and the protein−hapten complexes allowed Schultz and Stevens to propose the presence of a catalytic histidine (His^{H96}) and glutamate (Glu^{H50}) hydrogen bonding to the C3 hydroxyl, which might act to enhance the rate of the rearrangement by increasing electronic density on the oxygen substituent.[7c]

While a preference for the concerted mechanism has been found for both the simple uncatalyzed Cope and oxy-Cope reactions, appropriately placed radical stabilizing substituents can shift the mechanism to a stepwise, diradical pathway. This has been shown by experiment and theory to be the case for the Cope reaction of 2,5-diphenyl-1,5-hexadiene (**10**).[17] Phenyl substituents at C2 and C5 cause a shift in the mechanism from a concerted process to a diradical mechanism through a cyclohexyl 1,4-diyl (**11**) (Figure 4), although this intermediate sits in a very shallow potential well. The oxy-Cope substrate **1** for the process catalyzed by antibodies AZ28g and AZ28m has the same pattern of phenyl substitution.

Transition structure stabilization by electron delocalization through the phenyl substituents can be very significant ($\Delta H^{\ddagger} =$ 21.3 kcal/mol for **10** and 33.5 kcal/mol for 1,5-hexadiene), but it is also strongly dependent on the conformation about the C−Ph bond. The plane of the phenyl substituent should coincide with the plane of the three closest carbons in the cyclohexyl framework (e.g., C1−C2−C3, with Ph attached at C2) for maximum stabilization. This is true for both diradical and concerted pathways. This factor has been explored as part of this study.

(10) Cope, A. C.; Hardy, E. M. *J. Am. Chem. Soc.* **1940**, *62*, 441−444.
(11) (a) Evans, D. A.; Golob, A. M. *J. Am. Chem. Soc.* **1975**, *97*, 4765−4766. (b) Evans, D. A.; Baillargeon, D. J.; Nelson, J. V. *J. Am. Chem. Soc.* **1978**, *100*, 2242−2244. (c) Evans, D. A.; Nelson, J. V. *J. Am. Chem. Soc.* **1980**, *102*, 774−782.
(12) (a) Paquette, L. A. *Angew. Chem., Int. Ed. Engl.* **1990**, *29*, 609−627. (b) Wilson, S. R. Anion-assisted sigmatropic rearrangements. *Org. React. (New York)* **1993**, *43*, 93−250. (c) Paquette, L. A. *Tetrahedron* **1997**, *53*, 13971−14020.
(13) For a review of experimental work, see: (a) Gajewski, J. J. *Hydrocarbon Thermal Isomerizations*; Academic Press: New York, 1981; pp 166−176. For an account of mechanistic controversies, see: (b) Houk, K. N.; Gonzalez, J.; Li, Y. Pericyclic Reaction Transitition States: Passions and Punctilios, 1935−1995. *Acc. Chem. Res.* **1995**, *28*, 81−90. For reviews of computational results, see: (a) Wiest, O.; Montiel, D. C.; Houk, K. N. *J. Phys. Chem. A* **1997**, *101*, 8378−8388. (b) Houk, K. N.; Beno, B. R.; Nendel, M.; Black. K.; Yoo, H. Y.; Wilsey, S.; Lee, J. K. *J. Mol. Struct. (THEOCHEM)* **1997**, *398*−*399*, 169−179.
(14) Wiest, O.; Black, K. A.; Houk, K. N. *J. Am. Chem. Soc.* **1994**, *116*, 10336−10337.
(15) Baumann, H.; Chen, P. *Helv. Chim. Acta* **2001**, *84*, 124−140.
(16) (a) Yoo, H. Y.; Houk, K. N.; Lee, J. K.; Scialdone, M. A.; Meyers, A. I. *J. Am. Chem. Soc.* **1998**, *120*, 205−206. (b) Haeffner, F.; Houk, K. N.; Reddy, Y. R.; Paquette, L. A. *J. Am. Chem. Soc.* **1999**, *121*, 11880−11884. (c) Evans, D. A.; Baliargian, D. J. *Tetrahedran Lett.* **1978**, 36, 3315−3318. (d) Steigerwald, M. L.; Goddard, W. A.; Evans, D. A. *J. Am. Chem. Soc.* **1979**, *101*, 1994−1997.
(17) Hrovat, D. A.; Chen, J.; Houk, K. N.; Borden, W. T. *J. Am. Chem. Soc.* **2000**, *122*, 7456−7460.

With transition structure energetics anticipated to be highly sensitive to phenyl group conformation, Schultz and co-workers have noted in the crystal structure of the hapten−AZ28m complex that the phenyl groups attached to the transition-state mimic are far from the optimimal conformation in the real transition state. Further, they noted that the close proximity of neighboring residues is likely to restrict rotation to the better, coplanar arrangement. The germline structure, AZ28g, which complements the shape of the hapten less well, can be anticipated to provide a bit more space for better positioning of the aromatic substituents.[7c]

Most recently, the AZ28-catalyzed oxy-Cope reaction of **1** was the subject of a theoretical study by the Kollman group.[8] They used RB3LYP/6-31G(d) calculations for the concerted pathway. The B3LYP structures were used to develop force field parameters for AMBER as needed for a study by molecular dynamics. The reactant, transition state, and product were each docked into both AZ28m and AZ28g. The dynamics calculations revealed that the motion of all three ligands was much greater when the ligand was bound in the active site of the germline antibody than in the mature antibody. In line with experimental observations, they found that, whereas the mature form binds the hapten more tightly than the germline antibody, the germline, a better catalyst, binds the concerted transition structure of the reaction more tightly than the mature antibody.

Dynamics calculations were also used to assess the effect of six antibody residue mutations associated with maturation. This revealed that Asn^{L34} is particularly important for catalysis. Mutating Asn^{L34} to Ala (in AZ28m, the mature form of the antibody) was calculated to decrease transition-state binding by 7.6 kcal/mol and hapten binding by 6.8 kcal/mol. The effect of the mutation on substrate binding was not calculated, so the effect on catalysis is not certain but likely to be a significant diminishment. The effects of this mutation were much less pronounced in the germline form of AZ28.

Previous experimental and theoretical work on the AZ28 system provides important understanding and insights but also leaves a number of questions unaddressed. Here, density functional theory has been used to calculate structures and energetics for both concerted and stepwise reaction pathways and to calculate theoretical isotope effects for comparison to experimental values. The impact of hydrogen bonding in the active site has been explored quantum mechanically, as has the effect of phenyl orientation on reaction energetics and the impact of solvation. Docking of conformationally flexible ligands into the active site of mature and germline forms of AZ28 was used to evaluate how reactive conformations of the reactant bind in the active site and how transition structures bind in the active site. The origins of stereoselectivity in the catalyzed process have been explored.

Computational Methods

The concerted and stepwise reaction pathways were studied using the B3LYP density functional[18] and the 6-31G(d) basis set in the Gaussian 98[19] package. All structures were fully optimized unless otherwise noted. Each stationary point was characterized by harmonic frequency analysis. Unless stated otherwise, energies include zero-point energy corrections (frequencies were unscaled). Open-shell singlet species were treated with unrestricted B3LYP/6-31G(d) by generating an initial guess wave function in which the HOMO and LUMO are mixed to lift the spatial degeneracy of the α and β orbitals. Constrained optimizations employed the redundant internal coordinate feature of Gaussian 98. Solvation computations employed single-point energy evaluations on the gas-phase B3LYP/6-31G(d) structures using the CPCM model.[20] Internal conformational searches on reactants and products were performed by using the Monte Carlo search routine with the Merck Molecular Force Field[21] in the Spartan software package.[22] Kinetic isotope effects were calculated from the free energies computed by Gaussian for each of the isotopomers of reactants and transition states. CHELPG charges were used to study the electron densities of the reactant and transition state.[23]

Docking studies were performed using two protein structures. One was derived from the protein−hapten complex of the affinity-matured antibody (1AXS) and the other from the protein−hapten complex for the germline antibody (1D6V[24]). These structures, derived from X-ray crystallographic data, are available from the Brookhaven Protein Databank.[25] In both cases, the hapten and all water molecules were removed, the dimer was separated, and the monomer, consisting of the H and L chains, was retained for docking. Using tools provided within the Autodock software package (version 3.0.5),[26] protons were added to nitrogen and oxygen atoms as appropriate to neutral pH, charges derived from the Amber force field were added to each atom, and solvation parameters were incorporated into the structure file. This file was further modified to ensure integral charges on all residues. The two protein structures generated by this procedure (affinity-matured and germline) were used as the basis for generating two additional structures in which Glu^{H35} is protonated. Geometric placement of the proton was carried out manually, and charges were assigned to the proton and adjusted on the carboxylate moiety by analogy to similar functionality in the Amber force field.

All ligands docked into the active site were created using PM3 semiempirical methods[27] for structure optimization and ab initio molecular orbital theory at the RHF/6-31G(d) level to assign CHELPG partial charges to all atoms. Docking was carried out using AutoDock (version 3.0.5). In all cases, a 22.5 Å box centered on the active site was used to define the region of exploration. A 0.25 Å grid spacing within that region generated a set of 753 571 points for computation of electrostatic and van der Waals potentials within the protein active site.

A total of 200 docking runs were carried out on each ligand−protein pair. Within each run, a genetic algorithm was used to generate approximately 250 000 trial configurations differing in the placement, orientation, and conformation of the ligand within the active site.

(18) (a) Becke, A. D. *J. Chem. Phys.* **1993**, *98*, 5648−5652. (b) Becke, A. D. *J. Chem. Phys.* **1993**, *98*, 1372−1377. (c) Lee, C.; Yang, W.; Parr, R. G. *Phys. Rev. B* **1988**, *37*, 785−789.
(19) Frisch, M. J.; Trucks, G. W.; Schlegel, H. B.; Scuseria, G. E.; Robb, M. A.; Cheeseman, J. R.; Zakrzewski, V. G.; Montgomery, J. A., Jr.; Stratmann, R. E.; Burant, J. C.; Dapprich, S.; Millam, J. M.; Daniels, A. D.; Kudin, K. N.; Strain, M. C.; Farkas, O.; Tomasi, J.; Barone, V.; Cossi, M.; Cammi, R.; Mennucci, B.; Pomelli, C.; Adamo, C.; Clifford, S.; Ochterski, J.; Petersson, G. A.; Ayala, P. Y.; Cui, Q.; Morokuma, K.; Malick, D. K.; Rabuck, A. D.; Raghavachari, K.; Foresman, J. B.; Cioslowski, J.; Ortiz, J. V.; Baboul, A. G.; Stefanov, B. B.; Liu, G.; Liashenko, A.; Piskorz, P.; Komaromi, I.; Gomperts, R.; Martin, R. L.; Fox, D. J.; Keith, T.; Al-Laham, M. A.; Peng, C. Y.; Nanayakkara, A.; Challacombe, M.; Gill, P. M. W.; Johnson, B.; Chen, W.; Wong, M. W.; Andres, J. L.; Gonzalez, C.; Head-Gordon, M.; Replogle, E. S.; Pople, J. A. *Gaussian 98*, Revision A.9; Gaussian, Inc.: Pittsburgh, PA, 1998.
(20) Barone, V.; Cossi, M. *J. Phys. Chem. A* **1998**, *102*, 1995−2001.
(21) (a) Halgren, T. A. *J. Comput. Chem.* **1996**, *17*, 490−519. (b) Halgren, T. A. *J. Comput. Chem.* **1996**, *17*, 520−552.
(22) Spartan 5.1.3 (Unix); Wavefunction, Inc., 18401 Von Karman Ave., Suite 370, Irvine, CA 92715.
(23) Breneman, C. M.; Wiberg, K. B. *J. Comput. Chem.* **1990**, 11361−11373.
(24) Data for the germline structure were taken from the revised data file for 1D6V.pdb dated 04/10/2000.
(25) Berman, H. M.; Westbrook, J.; Feng, Z.; Gilliland, G.; Bhat, T. N.; Weissig, H.; Shindyalov, I. N.; Bourne, P. E. *Nucleic Acids Res.* **2000**, *28*, 235−242.
(26) Morris, G. M.; Goodsell, D. S.; Halliday, R. S.; Huey, R.; Hart, W. E.; Belew, R. K.; Olson, A. J. *J. Comput. Chem.* **1998**, *19*, 1639−1662.
(27) (a) Stewart, J. J. P. *J. Comput. Chem.* **1989**, *10*, 209−220. (b) Stewart, J. J. P. *J. Comput. Chem.* **1989**, *10*, 221−264.

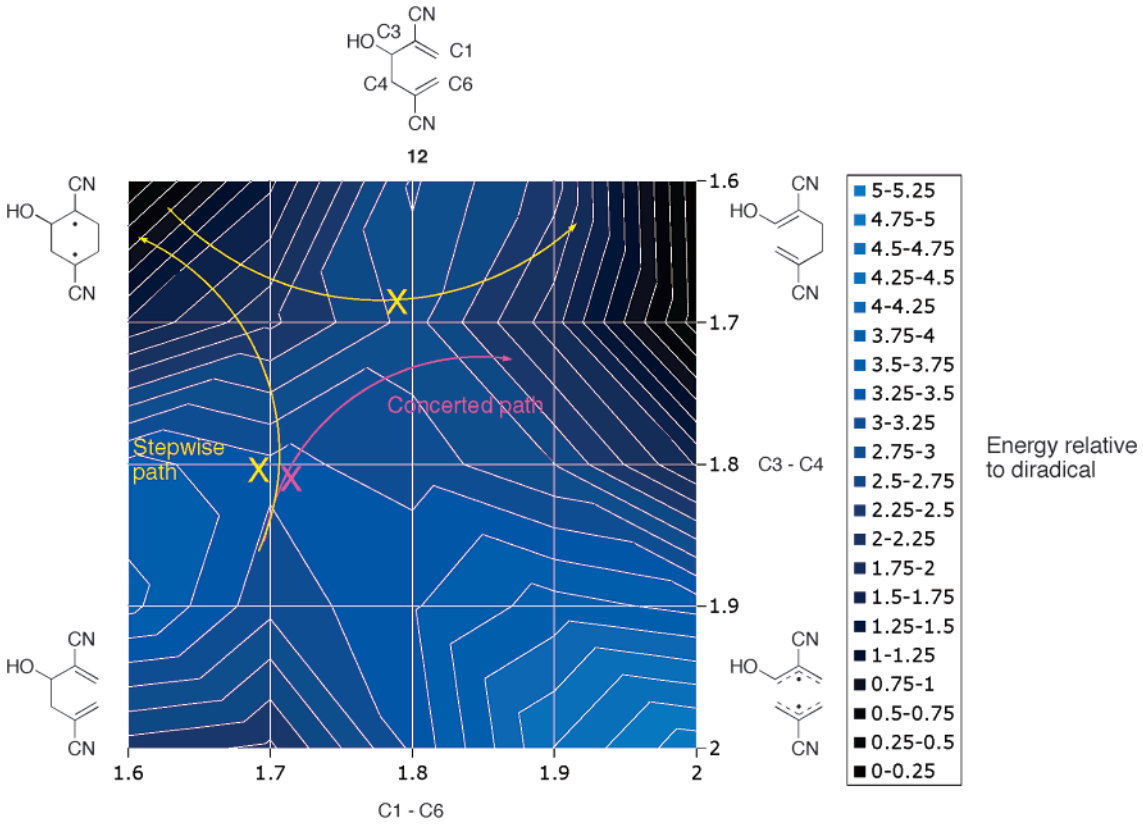

Figure 5. UB3LYP/6-31G(d) energy profile for the rearrangement of **12**. Crosses indicate the likely position of relevant transition states.

Conformational freedom was defined by specifying bonds which were to be torsionally active. In some experiments, a Gaussian potential energy function was applied as a torsional constraint on the C−Ph bond to bias the system to adopt the transition-state conformation.

The 200 final docked conformations generated for each ligand−protein pair were subjected to structural and energetic analysis using the clustering tools of Autodock, the structure and energy binning capabilities of Macromodel, and independent geometric analysis of specific structural interactions between the protein and the ligand.

Results and Discussion

Quantum Mechanics. Density functional theory using the B3LYP/6-31G(d) method was used to study the noncatalyzed oxy-Cope rearrangement of **1a** and **1b**. This method has previously been shown to be reliable at predicting the energetics of pericyclic reactions.[13,14,28]

To understand the effect on the oxy-Cope process of introducing radical-stabilizing substituents at the 2 and 5 positions of the hexadiene, the conformationally simpler model compound **12** (2,5-dicyano-1,5-hexadien-3-ol) was studied in depth. A recent study investigated the electronic structures of transition states of the parent Cope rearrangement of hexadiene and rearrangements of various cyano derivatives. For the parent, the weights of aromatic and diradical components were approximately equal.[29a] A UB3LYP/6-31G(d) energy profile defined by the two forming and breaking C−C distances was computed (Figure 5). The equivalent RB3LYP/6-31G(d) surface was also generated and is included in the Supporting Information. The concerted and stepwise paths are closely coupled. In fact, the transition state has a restricted electronic structure, and on the RB3LYP surface, it links the reactant directly to the product. However, on the UB3LYP surface, movement toward product links the transition state to the open-shell 1,4-diyl intermediate. This intermediate is linked to the product through a second transition state, which is an open-shell structure. However, the shape of the UB3LYP surface is such that, even though the path of steepest descent passes through the diradical, trajectories which bypass this intermediate may exist along the section marked "Concerted path" in Figure 5.

The closed-shell transition structure **13** is at 24.9 kcal/mol relative to reactant, while the diradical **14** is at 22.0 kcal/mol and the second open-shell transition structure **15** is at 24.2 kcal/mol. It can be seen in Figure 6 that the two transition states resemble the transition state computed for the stepwise Cope rearrangement of 2,5-dicyano-1,5-hexadiene, which has a forming bond distance of 1.832 Å and a breaking bond distance of 1.683 Å.[29b]

Subsequently, it proved possible to optimize the equivalent set of structures for the carboxylic acid-substituted substrate **1a**. The full set of structures was optimized for the case in which the hydroxyl substituent is placed axially, since preliminary calculations indicated this to be the lower energy isomer. The first transition structure is again closed-shell; **16** is 26.1 kcal/mol above the reactants, the diradical **17** is at 22.3 kcal/mol, and the second open-shell transition structure **18** is at 25.9 kcal/mol. These structures all resemble those for the model system

(28) Guner, V.; Khuong, K. S.; Leach, A. G.; Lee, P. S.; Bartberger, M. D.; Houk, K. N. *J. Phys. Chem. A* **2003**, *107*, 11445−11459.
(29) (a) Blavins, J. J.; Cooper, D. L.; Karadakov, P. B. *J. Phys. Chem. A* **2004**, *108*, 194−202. (b) The Cope rearrangement for 2,5-dicyano-1,5-hexadiene is degenerate and, therefore, the intermediate is flanked by two transition states which are related by symmetry; these are identical in structure and energy and correspond to a transition state into and a transition state out of the diradical intermediate.

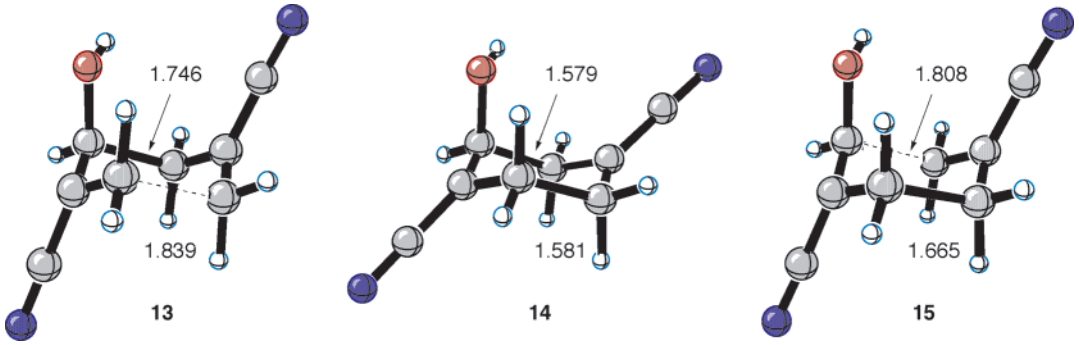

Figure 6. B3LYP/6-31G(d) optimized closed-shell transition state (**13**), diradical intermediate (**14**), and open-shell transition state (**15**) for the rearrangement of **12**.

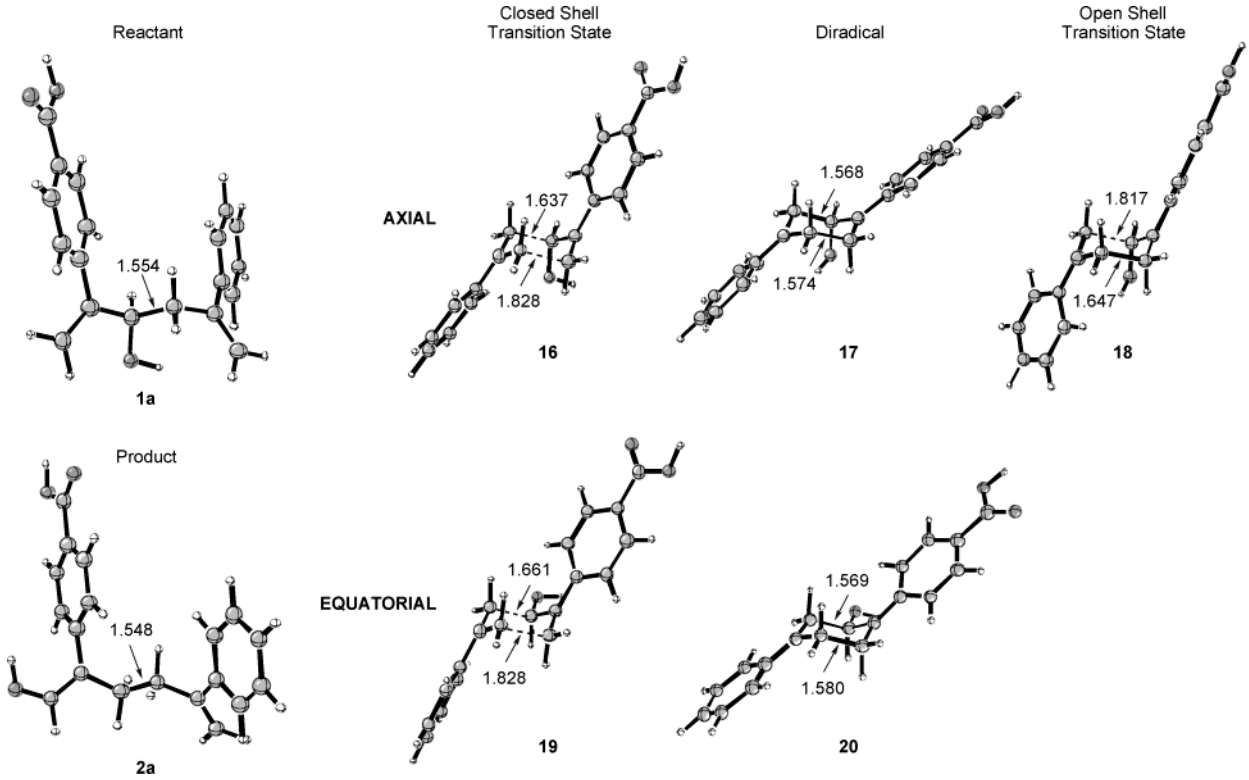

Figure 7. B3LYP/6-31G(d) optimized structures for the rearrangement of **1a**.

very closely and therefore suggest that the mechanism is the same (Figure 7).

It is likely that the mechanism computed above will hold for each of the other cases: the rearrangement of **1a** with an equatorial hydroxyl and the rearrangements of **1b** with the hydroxyl both axial and equatorial. The first transition state, which was rate-limiting, was therefore optimized for these three other options. With one exception, the breaking and forming bond lengths of this transition state were similar to those in **16**. The exception is the rearrangement of the anionic substrate **1b** with an axial hydroxyl. In this case, the closed-shell transition structure **21** was much more synchronous, and it is presumed that in this case the open-shell and closed-shell transition states are so compressed that they merge. The closed-shell transition structure **19** for the rearrangement of **1a** in which the hydroxyl substituent was equatorial was at 26.9 kcal/mol relative to reactants and therefore 0.8 kcal/mol higher than that with the hydroxyl axial. By contrast for the reaction of **1b**, the closed-shell transition state with an axial hydroxyl group, **21**, was at 25.6 kcal/mol relative to reactants, while that with an equatorial hydroxyl group, **23**, was at 24.6 kcal/mol, such that equatorial is favored by 1 kcal/mol (Figure 8).

The preference for an axial hydroxyl was observed in the optimized diradicals. For the carboxylic acid-substituted substrate **1a**, the diradical with an axial hydroxyl group, **17**, is at 21.9 kcal/mol, while that with an equatorial hydroxyl, **20**, is at 22.5 kcal/mol. For **1b**, the axially substituted diradical **22** is at 21.4 kcal/mol and the equatorially substituted diradical **24** is at 22.1 kcal/mol. Although there is generally an axial preference for the hydroxyl group in these structures, axial and equatorial configurations are close in energy. The axial preference arises because the partial double bond character between the aromatic ring and the cyclohexane framework causes $A_{1,3}$ strain to arise when the hydroxyl is in the equatorial configuration.

The NMR studies of Driggers et al. revealed that substrate **1** adopts a conformation in the antibody binding site in which the two termini of the substrate are held in close proximity.[7c] Presumably this conformation resembles and leads to the cyclic

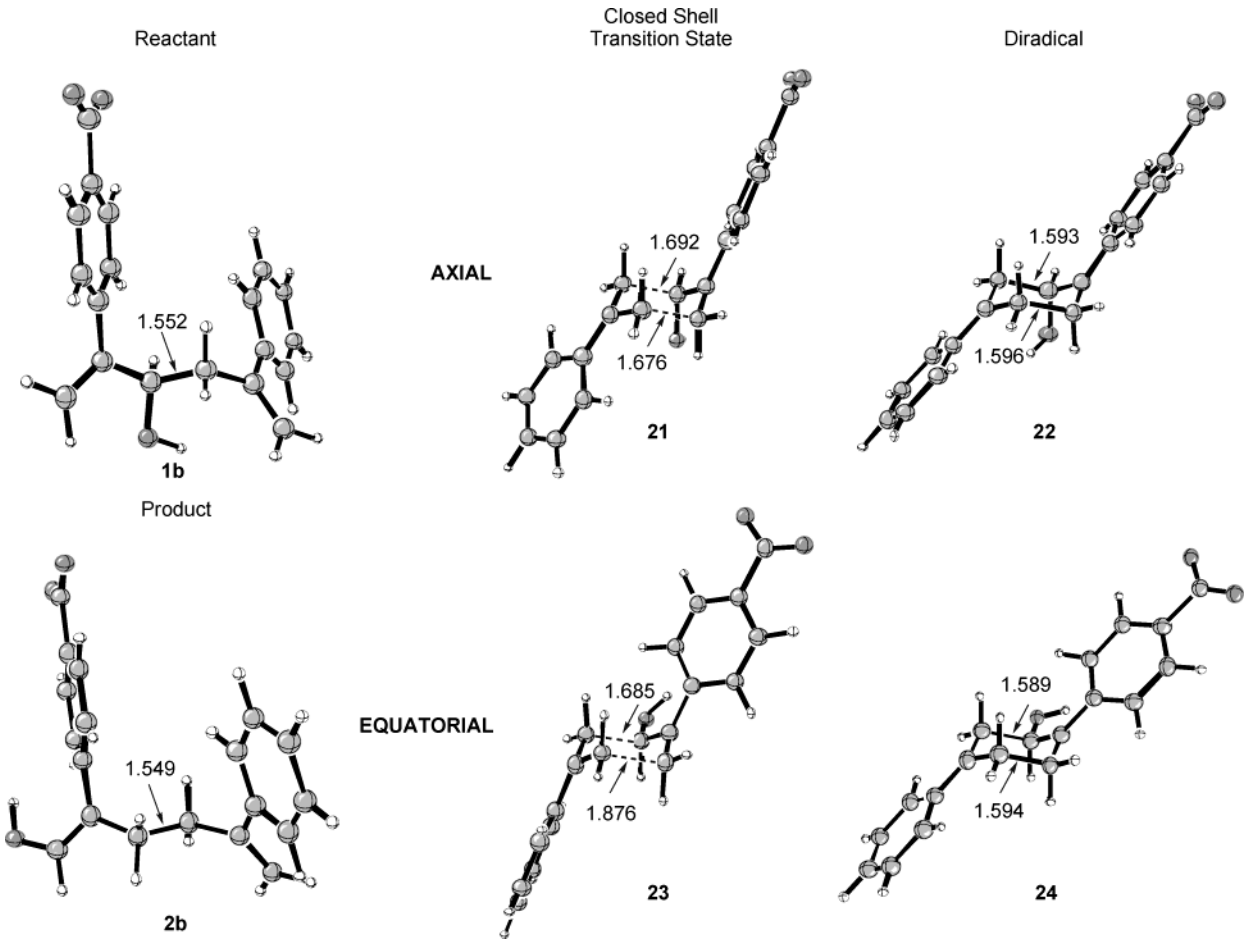

Figure 8. B3LYP/6-31G(d) optimized structures for the rearrangement of **1b**.

transition structure. To investigate the energetic penalty of adopting such a conformation, a constrained optimization was performed for the acid-substituted reactant **1a**, in which the C1−C3−C4−C6 dihedral was constrained to be 0° (Figure 9). The conformation shown as **25**, in which the hydroxyl is in a pseudo-equatorial position, is 0.6 kcal/mol above the minimum energy conformation of **1a** (no zero-point correction is included in this case because the constrained structure is not a genuine minimum). The conformation shown as **26**, in which the hydroxyl is in a pseudo-axial position, is 1.6 kcal/mol higher in energy than the lowest energy conformation of **1a**. The C−C distance for the bond that will be formed in the oxy-Cope rearrangement is 4.441 Å in **25** and 4.338 Å in **26**, considerably closer than in the minimum energy conformation, where they are 5.433 Å apart. These separations are consistent with the conformations in the active site that must be adopted if the experimentally observed NOEs are to be correct. These NMR measurements suggest that, in the active site, the alkene termini should be within 5 Å of one another.[7c]

Experimentally observed KIEs provide a sensitive probe of geometry in the real transition state of the reaction. If KIEs computed for the theoretically obtained transition structures match experimental values, this provides strong evidence suggesting that the calculated structures resemble the real structures. KIEs were calculated on the basis of the closed-shell transition state **16** for substrate **1a**, as this is the rate-limiting transition structure. The closed-shell transition state is the highest point on both the concerted and stepwise paths, and the KIEs are not, therefore, sufficient to distinguish the two paths, although the UB3LYP predicts that a stepwise path with a shallow intermediate is followed.

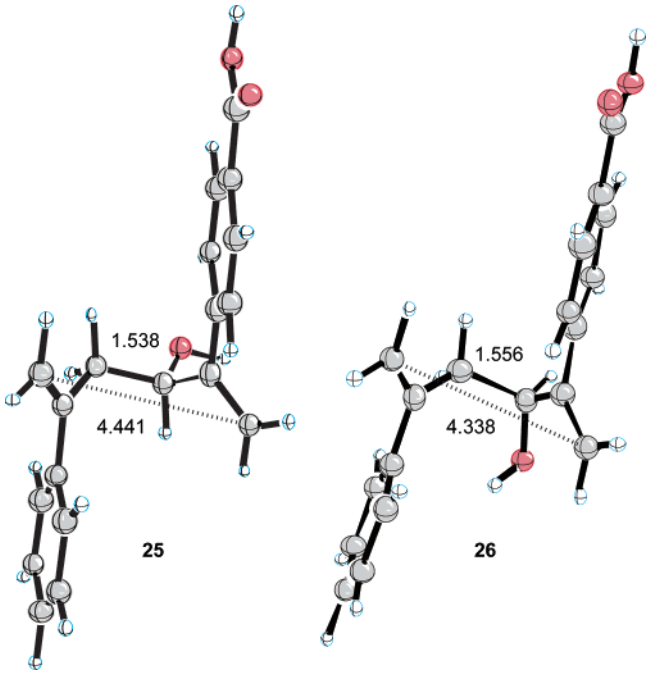

Figure 9. Two constrained conformations of **1a** in which the C1−C3−C4−C6 dihedral is fixed at 0°.

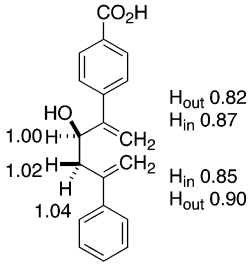

Figure 10. Individual kinetic isotope effects (k_H/k_D) computed for monodeuteration of **1a**.

Computation of the free energies of activation for **1a** passing through the transition state **16** and the isotopomers corresponding to **5** and **6** (with CO_2H in place of CO_2Me) permitted the kinetic isotope effects to be calculated. Fully protic **1a** is computed to react slower than the dideuterated carboxylic acid equivalent of **5** by a factor of 0.77 and slower than tetradeuterated **6** by a factor of 0.59. These are in very good agreement with the experimental values of 0.72 and 0.61, and provide evidence that transition structure **16** is a reasonable model of the real transition state, and confirm the claim that these isotope effects are consistent with the sigmatropic shift being the rate-limiting process.[7c] The factors by which **1a** is computed to react faster than monodeuterated species for the various hydrogens in **1a** were also calculated, and these are shown in Figure 10.

Calculations of solvation energies were performed on both the carboxylic and carboxylate systems with the CPCM model and water as the solvent.[20] The carboxylic acid **1a** is computed to have an energy of activation of 25.1 kcal/mol for the axial transition state **16** and 25.4 kcal/mol for the equatorial transition state **19** in water. Relative to the gas-phase calculations, the activation barrier is lowered by 1.0 kcal/mol for the lowest energy axial transition state. The equatorial transition state is solvated slightly more strongly, such that the preference for the axial transition state is diminished from 0.8 to 0.3 kcal/mol. The carboxylate reactant **1b**, as expected for a charged species, is computed to be more sensitive to solvation. The activation energy corresponding to the axial transition state **21** is computed to be 28.7 kcal/mol, and that for the equatorial transition state **23** is 29.1 kcal/mol. In the gas phase, a preference of 1.0 kcal/mol for equatorial was calculated, but solvation reverses the preference and axial is preferred by 0.4 kcal/mol. The barriers are raised compared to those in the gas phase by 3.1 and 4.5 kcal/mol for axial and equatorial, respectively. These calculations suggest that both ionized and neutral reactants prefer to rearrange through a transition state with an axial hydroxyl in the uncatalyzed aqueous reaction but that such a stereochemical preference is small and may be reversed in the less polar environment of the antibody. They further suggest that **1a** will rearrange more rapidly in a less polar environment and **1b** less rapidly. The degree of such medium-induced accelerations has previously been observed to be overestimated by similar solvation models.[30]

X-ray crystallography of the AZ28 antibody−hapten complexes revealed several hydrogen bonds involving the ligand C3 hydroxyl group. Among these, two involving histidine (His^{H96}) and glutamate (Glu^{H50}, by way of a linking water molecule) have been proposed by Schultz et al. to enhance the rate of the rearrangement by increasing electronic density on the oxy substituents.[7d]

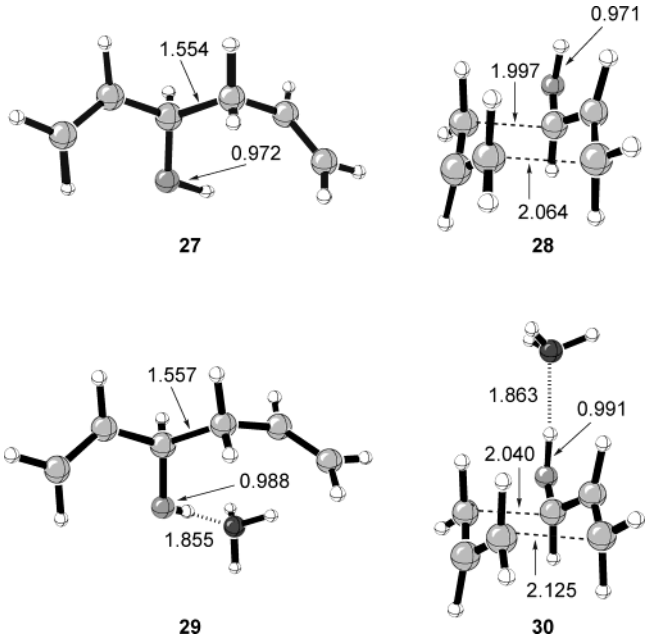

Figure 11. Substrate and transition structures for the oxy-Cope rearrangement of 3-hydroxy-1,5-hexadiene with and without hydrogen-bonded ammonia.

To study the effects of hydrogen bonding to the hydroxyl at C3 on the energy of activation of the rearrangement, the effect of an ammonia molecule accepting a hydrogen bond from the 3-OH of 3-hydroxy-1,5-hexadiene was studied. Hexadiene **27** has previously been computed to rearrange through a closed-shell concerted pathway involving the transition state **28**.[15] The oxy-Cope rearrangement of **27** has an energy of activation of 33.4 kcal/mol. The bond-forming and bond-breaking distances in transition state **28** are 2.064 and 1.997 Å, respectively. An ammonia molecule was placed to hydrogen bond to the hydroxyl at C3. An initial hydrogen-bonding angle of 180° and a distance of 2.8 Å were used; constraints were released and the structure was fully optimized and corrected for zero-point energy. The hydrogen-bonded complex of the reactant, **29**, has an N−H distance of 1.855 Å, and the complex of the transition state, **30**, has an N−H distance of 1.863 Å (Figure 11). The hydrogen bond lowers the energy of activation by 2.1 kcal/mol to 31.3 kcal/mol. The bond-breaking and bond-forming distances in the transition state are also affected. There is an increase in bond-breaking and -forming distances by 0.043 and 0.061 Å, respectively. CHELPG charge calculations show a localization of charge on the oxy substituent, which is the proposed cause of the rate acceleration of the rearrangement. The observed acceleration of the rearrangement is in agreement with previous work by Evans and Goddard, who have shown similar results for the anionic oxy-Cope system.[16] Baumann and Chen also found that, whereas the hydroxyl present in the oxy-Cope rearrangement lowers the barrier compared to the all-carbon Cope rearrangement slightly (by ~2 kcal/mol), deprotonation of the hydroxyl lowers the barrier by a great deal more (by 27 kcal/mol).[15] The hydrogen bond has a relatively minor effect.

Schultz et al. have proposed that the C2 and C5 phenyl substituents are forced into an unfavorable conformation in the

(30) Leach, A. G.; Houk, K. N.; Reymond, J.-L., unpublished results.

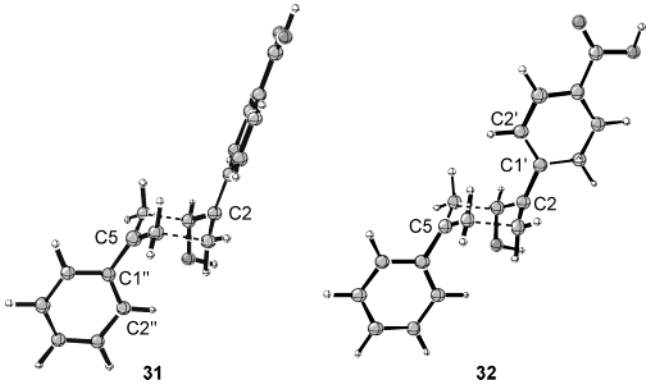

Figure 12. Transition-state geometries with constrained phenyl group conformation.

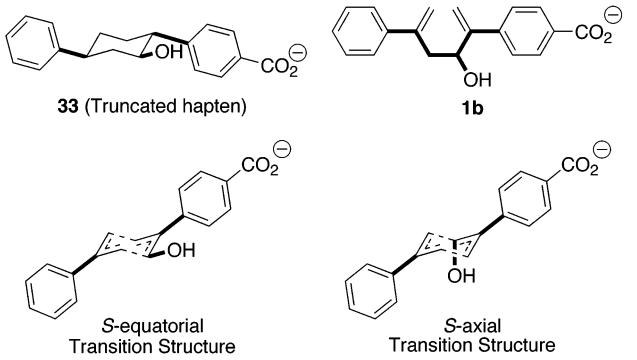

Figure 13. Ligand isomers for docking studies. Bonds that are considered as torsionally active in the flexible docking are indicated in bold.

mature antibody.[7c] To assess the energetic penalty associated with poor phenyl group conformation, two constrained B3LYP/6-31G(d) optimizations were performed on the basis of transition state **16**. In the first, the phenyl group was constrained such that the C2−C5−C1″−C2″ was 0°, in effect placing the π system orthogonal to a radical at the adjacent C5, thereby prohibiting any significant electron delocalization in the π system (Figure 12). To simplify the calculation, the C1−C6 and C3−C4 distances were constrained to the same values they have in **16**. The resulting structure **31** is 7.2 kcal/mol above **16**. In the second optimization, a fourth constraint was added to those used for **31**: the C5−C2−C1′−C2′ dihedral was also constrained to be 0°. This places both the phenyl group and the carboxylic acid-substituted phenyl group orthogonal to any adjacent radical. The resulting structure **32** is 15.8 kcal/mol higher in energy than **16**. This confirms the very important sensitivity of transition structure energetics to phenyl group conformation.

Ligand−Antibody Docking. Having used DFT to establish gas-phase ligand structures and energetics along the reaction coordinate, as well as the effects of solvation, hydrogen-bonding, and phenyl conformations, attention was turned to how these same structures interact with the active site of AZ28. Docking experiments were designed to explore several issues, including the greater catalytic activity of the germline structure, how the phenyls get in the conformation required for a reactive transition structure, how substrate binding allows for hexadiene termini to achieve reasonable proximity in the active site, and what is the origin of the 15:1 *S* stereoselectivity of the mature form of AZ28.

Four protein structures were employed in this study. The first, AZ28m, is the mature form of AZ28, with the standard protonation states applied as expected at pH 7. Examination of the active site of the antibody revealed that two carboxylates, Glu^{H35} and Glu^{H50}, are in very close proximity. For both to be deprotonated is unlikely, particularly in the relatively nonpolar environment inside the active site. Consequently, a second antibody structure was generated by protonating the more deeply buried of these two residues (Glu^{H35}). This form of the antibody is denoted AZ28m−H throughout.[31] The same two residues are present in the germline antibody, and the same scheme of protonating the more deeply buried residue (Glu^{H35}) was implemented. Thus, all docking trials were also carried out with two forms of the germline antibody, AZ28g and AZ28g−H.

A total of seven ligands were docked into the active site of each of the four antibody structures described above. These seven included a core of the hapten (**33**) as a preliminary check on methodology, four different isomers of the transition state, and both enantiomers of the starting diene. The four transition-state structures include those derived from both *R* and *S* stereoisomers, and then for each enantiomer the two possible cyclic configurations, one with the hydroxyl axial and the other with the hydroxyl equatorial. Representative structures are provided in Figure 13. Whereas the hydroxyl would be slightly favored in the equatorial position in cyclohexanol, the quantum mechanics results of this study show that, to avoid steric interactions with the phenyl group, the hydroxyl in the dehydrocyclohexyl exhibits much more mixed behavior, often favoring the axial orientation. It is of note that the small intrinsic preferences in the orientation of the hydroxyl group could easily be compensated for by a particularly effective binding mode in the active site.

The geometries of the basic ligand structures used in docking were generated with the PM3 method, since the docking experiments were performed contemporaneously with the DFT calculations. The geometries generated by PM3 are similar to those generated by B3LYP. The flexible ligand docking methodology of Autodock is based on selection of specific ligand bonds, about which the structure has torsional freedom. These ligand bonds for **33**, **1b**, and a general version of the transition structure (illustrated by the *S* stereoisomer) are indicated in bold in Figure 13.

The four transition-state models required further consideration. The quantum mechanics results showed clearly that electron delocalization and stabilization of the transition state requires the phenyl groups to be close to coplanar, with the three carbons in the cyclohexyl framework closest to that phenyl group. Without a constraint on the C−Ph bond, the transition structure model as treated by the simple force field of Autodock adopts a lowest energy conformation with the phenyl group effectively bisecting that three-carbon plane (Figure 14).

For this reason, each of the four transition-state models was docked into the active sites twice, once with the phenyl groups freely rotating and a second time with a Gaussian energy function applied from within Autodock to bias the ligand to have the plane of the phenyl groups close to coplanar with the allyl fragment, as required for real transition structure reactivity. This resulted in the phenyl group being about 19−21° out of

(31) As can be seen in Figure 15a, the proton on the carboxylate of Glu^{H35} is pointed directly toward one of the carboxylate oxygens of Glu^{H50}, with a distance between them of 1.63 Å.

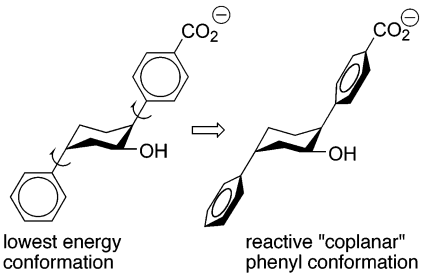

Figure 14. Docked conformers of transition structure.

the plane of the allyl carbons, and this is similar to the optimal orientation as determined by DFT in the gas phase (~15° displacement from coplanarity).

While the docking studies described below generated a number of bound configurations, four principal binding modes were identified. These are most easily defined by the active site residue to which the ligand hydroxyl is hydrogen bonded. The four principal residues observed by these docking experiments to form this hydrogen bond are Glu^{H35}, His^{H96}, Asp^{H101}, and Tyr^{H100a}. Glu^{H35} and His^{H96} are near each other along one side of the active site pocket. X-ray crystallography shows the hydroxyl of the hapten bonding to His^{H96} (and to the nearby Glu^{H50} which hydrogen bonds through a water molecule link).[7d] Glu^{H35} is just slightly deeper in the active site and, for our transition-state models, serves as the alternative and primary binding locus on that side of the active site. This may be due to the lack of the tether, allowing deeper penetration into the pocket by the simplified hapten model compound, and in the case of the transition structure models it is probably due to the somewhat shorter structure relative to the hapten. In both cases this brings the OH just a bit deeper in the pocket, and consequently in better alignment with Glu^{H35}. Interestingly, Glu^{H35} is the carboxylate we chose to protonate. While this results in somewhat reduced charges on this residue in the protonated forms of the antibody, it still serves as the principal hydrogen bonding site on that side of the active site according to these docking studies. This mode of binding is illustrated in Figure 15a, in which the lowest-energy docked configuration for the truncated hapten model (green) is shown along with a rendition of the hapten (white) as positioned by X-ray crystallography for comparison. The view in Figures 15 and 16 is looking directly into the active site.

A principal result of this study is most easily characterized by a second locus for possible hydrogen bonding of the ligand OH in the active site. Asp^{H101} and Tyr^{H100a} are on a side of the active site well separated from the Glu^{H35}−His^{H96} pair described above. Asp^{H101} is the more deeply buried of the two residues, which are also in close proximity to Ser^{L34} in the germline structure and to Asn^{L34} in the affinity-matured antibody. Several ligand structures were found by this study to be preferentially hydrogen bonded to this side of the active site pocket, and specifically to Asp^{H101}, as will be presented below. This second binding motif is illustrated by using the simplified hapten model in Figure 15b, again with a background rendition of the hapten as found by X-ray analysis. It is of note that the second mode is achieved, while leaving phenyl groups positioned similarly, by the cyclohexyl core rotating approximately 180° on the axis of the two phenyl groups.

A summary of the results of the docking experiments is presented in Tables 1−4, generally listing in order (1) the form of the antibody, (2) the binding mode of the ligand identified by the residues to which the C3 hydroxyl group hydrogen bonds, (3) the number out of 200 docking runs that resulted in this particular docking mode,[32] and (4) the mean docked energy (MDE in kcal/mol) for the structures involving that binding mode.[33]

Results from docking hapten model compound **33** into each of the four protein structures (Table 1) provide a check of the Autodock methodology and force field. This study would predict the hapten to preferentially adopt a binding mode with hydrogen bonding to Glu^{H35} and His^{H96}. This placement matches that determined by X-ray crystallography very well, with the hapten just slightly deeper in the pocket (see Figure 15a). This mode was also found in the molecular dynamics work of Asada et al. for binding of the hapten into the mature form of the antibody.[8] Two important observations should be noted. First, the protonation state of Glu^{H35} has very little influence on either the partitioning between docking modes or the relative binding energy of those docked configurations (typically within 0.1−0.2 kcal/mol). This pattern holds throughout this study. Thus, for the sake of brevity, we report in subsequent tables docking data for only the protonated antibodies, AZ28m−H and AZ28g−H. One deviation in the behavior of the unprotonated and protonated systems is noted in a footnote to Table 2.

The second feature of note in these data is the appearance of the alternate binding mode discussed above. In the case of docking with the mature antibody, whether AZ28m or AZ28m−H, the Glu^{H35}−His^{H96} docking mode is computed to be the lowest in energy, but more docking runs generated the energetically very close alternative binding mode, with the hydroxyl group bonded to Tyr^{H100a} on the other side of the active site pocket (Figure 15b). The Glu^{H35}−His^{H96} docking mode is very close to that found for the hapten in the crystal structure, while the alternative Tyr^{H100a} docking mode leaves the two aromatic rings in the same basic position, but with the cyclohexane ring effectively rotated 180° on the axis provided by the two phenyl substituents, such that the protruding hydroxyl group can now form a hydrogen bond to a residue on the opposite side of the active site pocket. With the germline structure, all 200 docking runs yielded a structure that closely matches that found by X-ray analysis. In line with the experimental K_D values, the hapten is computed to bind more strongly with AZ28m than with AZ28g, although the difference is less than expected from the K_D's which is ~2 kcal/mol. It is possible that having two energetically close docking modes provides an entropic advantage to binding the hapten with AZ28m compared to AZ28g, further enhancing its binding ability.

Having established that the docking methodology is capable of reproducing the experimental observations concerning binding of the hapten, we next turned our attention to the interaction of the transition structures with the four protein structures. The

(32) For clarification, 200 docking runs were carried out on each antibody−ligand pair, with each run generating a final, lowest energy configuration. Of those 200 runs, those which generated an essentially identical binding mode and geometry were clustered as an ensemble of like structures, and the number of structures in the cluster along with the mean docking energy is reported.

(33) Autodock provides an estimate of the free energy of binding, which is based on the mean docking energy we report but also includes corrections based on the conformational degrees of freedom in the ligand. We report the mean docking energy, which takes into account all ligand−protein interactions (van der Waals, electrostatic), because of complications from our placing additional conformational restrictions on the transition-state models.

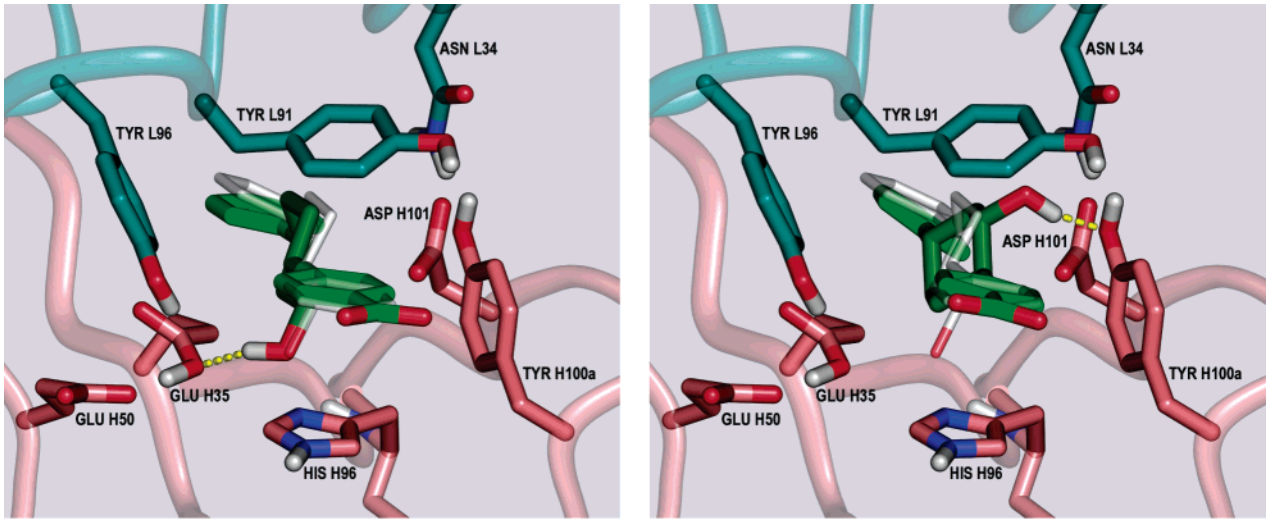

Figure 15. Two typical binding modes of *S*-equatorial-hapten model **33** in AZ28m−H. (a) Hydrogen bonding to Glu^{H35}; (b) hydrogen bonding to Tyr^{H100a}.

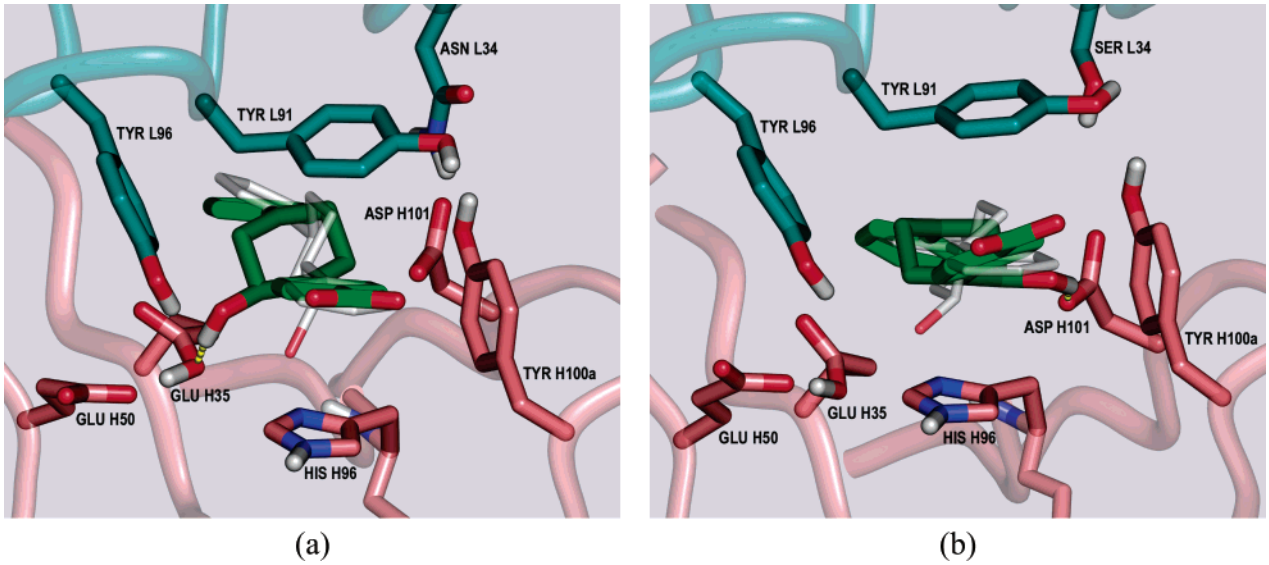

Figure 16. Two typical binding modes found for torsionally constrained transition states. (a) *S*-equatorial with AZ28m−H; (b) *R*-equatorial in AZ28g−H.

Table 1. Docking Results for the Hapten Model **33**

protein	binding mode	no./200 runs	MDE (kcal/mol)
AZ28m	Glu^{H35} and His^{H96}	55	−12.1
	Tyr^{H100a}	135	−11.6
AZ28m−H	Glu^{H35} and His^{H96}	71	−12.2
	Tyr^{H100a}	126	−11.9
AZ28g	Glu^{H35} and His^{H96}	200	−11.4
AZ28g−H	Glu^{H35} and His^{H96}	200	−11.4

structures were initially docked with no specific torsional constraint on the C−Ph bond. The binding modes generated with this approach all have the phenyl rings more or less bisecting the approximate plane of the cyclohexyl ring, much like in the hapten model. This is not a realistic conformation for the actual transition structures, but an interesting amplification of hapten results can be seen in the data. While the bonding mode to Glu^{H35} is represented, alternate binding modes appear, and in particular binding to Asp^{H101} on the other side of the active site is a dominant mode of binding. Interestingly, the hydroxyl in an equatorial position seems to favor the Glu^{H35} binding site, while the axial orientation seems better able to bond to the Asp^{H101} on the other side of the active site. The axial hydroxyl conformation is not available to the hapten, but it could certainly be generated as the cyclic transition structures form. Binding is again a bit tighter in the mature form, and the *S*-axial form is particularly well situated to bind to the Asp^{H101} residue.

Biasing the phenyl groups to adopt a conformation close to that determined as optimal by quantum mechanics generated a new data set and forces considerable geometric change in ligand binding configuration. In these studies, the aromatic rings were typically ∼20° away from coplanarity with the adjacent three-carbon fragment in the cyclohexyl ring. The results for each of the four ligand isomers docked into the protonated antibody structures are given in Table 3, and the protonation state of Glu^{H35} was again computed to have little influence on either the docking modes or the relative energetics.

Bonding to Glu^{H35} is a bit more common for these transition structure mimics in the mature form of the antibody. However, the Asp^{H101} mode is important and, in fact, dominant in the germline catalyst. This is an interesting distinction between the

Table 2. Docking Results for Unconstrained Transition Structure Model

	AZ28m–H			AZ28g–H		
hexadiene isomer	binding mode	no./200 in cluster	MDE (kcal/mol)	binding mode	no./200 in cluster	MDE (kcal/mol)
S-equatorial	Glu^{H35}	135	−13.45	Asp^{H101}	193	−12.78
S-axial	Asp^{H101}	167	−13.43	Asp^{H101}	185	−12.78
R-equatorial	Glu^{H35}	200	−13.89	Glu^{H35}	141	−12.87
				Tyr^{H100a}	59	−12.47
R-axial[a]	no H-bond	41	−13.11	Asp^{H101}	48	−12.48
	Asp^{H101}	91	−12.95	Asp^{H101}	142	−12.22
	Glu^{H35}	42	−12.91			

[a] In the unprotonated mature form (AZ28m), the *R*-axial isomer docked with less variation in modes to yield a single dominant cluster (Glu^{H35}, 50 runs, −12.84 kcal/mol). Two Asp^{H101} modes are reported for the *R*-axial isomer docking into AZ28g−H as the geometric placement varied just slightly between these two clusters.

Table 3. Docking Results for Constrained Transition Structure Model

	AZ28m–H			AZ28g–H		
hexadiene isomer	binding mode	no./200 in cluster	MDE (kcal/mol)	binding mode	no./200 in cluster	MDE (kcal/mol)
S-equatorial	Glu^{H35}	94	−11.52	Glu^{H35}	24	−11.11
				Asp^{H101}	169	−10.85
S-axial	Asp^{H101}	21	−11.07	Asp^{H101}	133	−10.54
	No H-bond	94	−10.22	Asp^{H101}	23	−10.40
R-equatorial	Glu^{H35}	54	−10.85	Asp^{H101}	158	−11.15
	Glu^{H35}	90	−10.46			
R-axial	Glu^{H35}	180	−11.10	Asp^{H101}	117	−10.87
				Glu^{H35}	61	−10.70

Table 4. Frequency of Constructive Binding Modes Observed for Each Protein−Ligand 1b Complex

protein	ligand **1b** stereochemistry	(A) general requirements	(B) close termini	(C) Glu^{H35}	(D) Asp^{H101}
AZ28m−H	*S*	120	50	10	17
	R	70	17	8	5
AZ28g−H	*S*	127	32	2	16
	R	128	43	2	22

two forms of the antibody, and the multiple modes support the dynamics results that the germline structure allows more freedom of positioning of the ligand.[8] However, in that molecular dynamics study, the binding mode to Asp^{H101} showed up specifically in the mature form of the antibody, not the germline structure. The results here suggest that, when it is available, even when binding into a rigid active site, it may well be the preferred hydrogen-bonding mode for the transition structure. Two typical docking modes, those for *S*-equatorial bonding to Glu^{H35} in the mature form of the antibody and *R*-equatorial bonding to Asp^{H101} in the germline protein, are illustrated in Figure 16.

In attempting to analyze the origin of the greater catalytic effect of the germline form of the antibody as opposed to the mature form, the significant errors in the Autodock docking energies (approximately ±2.0 kcal/mol) and the small energetic difference observed experimentally (the K_{TX} values indicate a difference in free energy of transition-state binding between the germline and mature forms of the antibody of 0.7 kcal/mol) prevent quantitative analysis of the results. In contrast to experimental observation, the tightest transition-state binding is computed for the mature form of AZ28, binding the *S*-equatorial isomer of the transition state.

The quantum mechanics study revealed that, for the anionic substrate **1b**, there is a 1 kcal/mol preference for the equatorial pathway in the gas phase. The interior of an antibody is relatively nonpolar, and consequently there is likely to be an inherent, if small, preference for the equatorial pathway. The germline form, which always prefers to bind the equatorial isomer of the transition state, may benefit from this. However, the studies of Asada et al. indicate that a docking study with a static protein structure may not be able to correctly differentiate the transition-state binding ability of the two proteins.[8] Their molecular dynamics simulations suggest that the greater flexibility of the side chains in the binding site of the germline antibody compared to the relatively more rigid side chains in the mature form enables the germline form to better accommodate the real transition state, which differs from the hapten particularly with respect to the flattening at the two carbons adjacent to the aromatic rings.

Turning to the stereoselectivity of the reaction, there is an experimentally observed preference for AZ28m to catalyze the reaction of the *S* isomer, which corresponds to a difference in activation free energy of approximately 1.6 kcal/mol. The mature form of the antibody is calculated to preferably bind the *S* stereoisomer of the transition structure with an equatorial −OH. The two axial isomers are less well and about equally bound, and the *R*-equatorial isomer is the least well complexed. The binding energy for the *S*-equatorial isomer is ∼0.5 kcal/mol greater than that for the *R*-axial isomer. This, combined with the inherent preference for equatorial (up to 1 kcal/mol), could account for much of the stereoselectivity. The germline antibody shows no such preference. The *R*-equatorial isomer seems to be a bit better bound than the *S*-equatorial isomer, and the same slight preference can be argued for the *R*-axial vs the *S*-axial isomer, but these differences are really beyond the accuracy of the force field to distinguish with confidence.

Another approach to understanding the stereoselectivity of the process is to consider the binding of the starting material, particularly as the ligand adopts a reactive conformation (or near-attack conformation[34]). The substrate is a conformationally highly flexible species, with six torsionally active bonds. This

(34) Lightstone, F. C.; Bruice, T. C. *J. Am. Chem. Soc.* **1996**, *118*, 2595−2605.

leads to a large number of conformations, each of which may bind into the protein in many competitive orientations. The docking runs produced many small conformational clusters with similar MDEs. Consequently, the results of the docking of the two stereoisomeric hexadiene substrates required more analysis than those obtained for the hapten or transition states. In this case, rather than focus just on energetics, an effort to more broadly assess geometric considerations led to the following results. First, a general filter was applied to the entire set of resulting structures from the 200 docking runs. This filter selected those that were in the active site with the correct global orientation (excluding those that have the carboxylate end deep in the active site) and which were within 3 kcal/mol of the lowest mean docking energy. Those structures meeting these requirements are tabulated in column A in Table 4. From this subset was found the number with hexadiene termini close enough ($\leq$4.5 Å) to ensure the structure would have a loose chair conformation as needed in advance of evolving into the transition structure (column B). Finally, from this set of reactive conformations were separated those that are hydrogen bonding to either Glu^{H35} or Asp^{H101} (columns C and D, respectively), anticipating that this may further support binding and transition-state formation. The results in Table 4 parallel very closely those for docking into the unprotonated antibodies.

This table shows that the mature form of the antibody is better able to bind the *S* stereoisomer of the substrate (120 *S*:70 *R*), even when no conformational constraint is present. This preference is enhanced (50 *S*:17 *R*) when considering only those conformations within the active site with reasonably close termini ($\leq$4.5 Å, in what may be called a near-attack conformation), and greater stereoselectivity (17 *S*:5 *R*) comes when considering those conformations which hydrogen bond to Asp^{H101} rather than to Glu^{H35} (10 *S*:8 *R*). By contrast, the germline form appears to offer little stereochemical distinction at the level of simply binding the two enantiomers of the reactant (127 *S*:128 *R*) but then exhibits modest selectivity for the *R* stereoisomer as we add the constraints that the termini be within 4.5 Å (32 *S*:43 *R*) and that there be hydrogen bonding to an active site residue (18 *S*:24 *R*). Interestingly, almost all of the near-attack conformations in the germline antibody active site involve ligand hydrogen bonding to the Asp^{H101} residue rather than to Glu^{H35}. To the degree that docking the substrate into the active site can shed light on possible pathways of reaction, the results above suggest two intriguing predictions. The first is that the germline structure should show less stereoselectivity than the mature form of the antibody and that it should favor reaction of the *R* isomer. Second is that, in the germline structure, Asp^{H101} is the preferred hydrogen-bonding locus for substrate as the ligand prepares for rearrangement. These results agree in outcome with what was found for binding of the conformationally constrained transition structures. While the mean binding energies of the clusters are not reported, they are typically $\sim$2 kcal/mol less than those found for the transition structures, as required for catalysis.

The docking studies reveal a complex interaction between active site and ligand, both as reactant first binds and then adopts a reactive transition structure conformation. One of the most intriguing results of this docking study is the indication that Asp^{H101} (and perhaps Tyr^{H100a} if the ligand does not get quite as far into the active site) is a primary site of hydrogen bonding. Interesting experimental support for this conclusion comes from the work of Stevens, Schultz, and co-workers.[7b] While investigating the relative importance of the six individual somatic mutations connecting the germline and affinity-matured structures toward ligand affinity and catalytic efficiency, they determined that one mutation was much more important than the others, $Ser^{L34} \rightarrow Asn$. This mutation only slightly increases binding affinity while significantly reducing catalytic activity. Similarly, mutation of Asn^{L34} back into Ser in AZ28m increases catalytic activity 20-fold. They suggest that the mutation has its effect on the catalysis by changing the shape of the active site. They point out that the Asn residue in the affinity-matured structure interacts directly with both Tyr^{H100a} and Asp^{H101}. This matrix of hydrogen bonds forms a wall on one side to the active site and modestly increases binding affinity for the hapten, but it also reduces significantly the conformational freedom for the bound ligand and specifically the cyclohexyl core and, therefore, its ability to achieve the very specific orientation of that core relative to phenyl substituents as required in the reactive transition structure.

The molecular dynamics work of Asada also highlights the importance of the $Ser^{L34} \rightarrow Asn$ mutation. Using alanine and glycine scanning methods, a residue replacement method which uses an existing trajectory and does not allow conformational changes, supports L34 as the most important of the somatic mutations. It is also the residue of this set closest to the active site.

The work reported here suggests that the Asp^{H101} carboxylate is a site of hydrogen bonding and a part of the catalytic mechanism, presumably by facilitating binding and by increasing electron density on the oxygen of the ligand. The $Ser^{L34} \rightarrow Asn$ mutation has a direct impact on this proposed mechanism. In the mature form of the antibody, the longer side chain of Asn^{L34} allows it to hydrogen bond directly to the Asp^{H101} carboxylate ($H^{Asn}-O^{Asp} \approx 2.5$ Å) and to the Tyr^{H100a} ($H^{Asn}-O^{Tyr} \approx 1.7$ Å). These links also pull the Asp^{H101} carboxylate into hydrogen-bonding distance with Tyr^{H100a} ($H^{Tyr}-O^{Asp} \approx 1.7$ Å). Thus, these residues do indeed create a three-way hydrogen-bonded lattice along one side of the active site, and the Asp^{H101} carboxylate is likely to be relatively tightly held in place by these two hydrogen bonds to neighboring residues.

In contrast, the shorter side chain of Ser^{L34} in the germline structure prevents it from hydrogen bonding directly to either Tyr^{H100a} ($H^{Ser}-O^{Tyr}$ distance $\approx$ 3.4 Å) or, more importantly, to Asp^{H101} ($H^{Ser}-O^{Asp}$ distance $\approx$ 4.0 Å). As a consequence, it also fails to bring Asp^{H101} and Tyr^{H100a} ($H^{Tyr}-O^{Asp}$ distance $\approx$ 3.7 Å) into hydrogen-bonding proximity. This leaves the carboxylate of Asp^{H101} much more available to serve as a catalytic residue by hydrogen bonding to the $-$OH in the ligand transition structure. The carboxylate's freedom is tempered in the germline$-$hapten complex, as X-ray analysis reveals a water molecule situated between these three residues, providing a hydrogen bond link between them. We do not know anything about the presence or absence of water in the active site during catalysis. However, even with a water present as with the hapten, the carboxylate should still have more freedom than in the affinity-matured structure. This result offers another possible explanation for the observed strong impact of this one particular somatic mutation.

Conclusions

A quantum mechanical study of the reaction catalyzed by the antibody AZ28 revealed that it follows a stepwise mechanism which is slightly preferred over the concerted. The closed-shell transition state is the highest point on the reaction pathway and hence will be responsible for the observed kinetic isotope effects. It continues to an intermediate diradical that can easily go on to product. Free energy calculations reveal that the difference in free energy of activation for the dideuterated and tetradeuterated isomers of the reactant used for experimental kinetic isotope effect measurements can reproduce the observed rate differences well and provides support for the computed transition structures and mechanism. Solvation in water is computed to lower the barrier to the reaction of the acid and raise the barrier to the reaction of the carboxylate.

The gas-phase reaction shows a preference for reaction through a transition state with an axial hydroxyl for the protonated substrate **1a** but a preference for an equatorial hydroxyl for the anionic substrate **1b**. Solvation causes both substrates to prefer an axial hydroxyl group. The antibody interior may be sufficiently nonpolar to more closely resemble the gas phase than the aqueous phase and hence prefer an equatorial hydroxyl. Rotation of the aromatic rings away from their optimum orientation carries with it a severe energetic penalty. Hydrogen bonding to the ring hydroxyl can lower the barrier to the oxy-Cope rearrangement. The structures obtained by quantum mechanics are pertinent to the uncatalyzed reaction, and the interaction between these structures and the protein will determine how the antibody catalyzes the reaction.

Flexible ligand docking reproduced the known X-ray crystal structure for hapten complexation, and calculation of the mean docking energy predicts stronger binding of the transition structures than starting materials, as required for catalysis. Not surprisingly, the simple force field model was not able to reproduce all of the complex and subtle features of the transition structure, as revealed by the quantum mechanics calculations, including the configurational preferences of the ligand hydroxyl group and phenyl group conformation. The docking results predict correctly the stereoselectivity of the process and suggest that the origins are in the initial binding of the ligand and the preference for the *S* isomer of the transition structure to be bound. With these results also comes the prediction that the germline antibody should be less selective and may actually favor the other enantiomer.

The second feature revealed through docking concerns the possible alternate hydrogen-bonding locus, and specifically binding to Asp^{H101}. Experimental work supports the importance of Asp^{H101} in the catalytic process, but it does not directly reveal the mechanism of its involvement. The docking results of this study suggest Asp^{H101} to be an important position of hydrogen bonding, particularly in the germline structure, and it may be a critical component in allowing the ligand to fold to a reactive conformation while achieving the required conformation of phenyl substituents.

Acknowledgment. We are grateful to the National Science Foundation for financial support of this research, to AstraZeneca and the UK Fulbright Commission for a fellowship to A.G.L., and to the Camille and Henry Dreyfus Foundation (Claremont), the National Science Foundation (UCLA), and the National Computational Science Alliance for the computer resources used in this work. This work is dedicated to Professor Elisheva (Chevy) Goldstein on the occasion of her retirement.

Supporting Information Available: Cartesian coordinates of all molecules and transition states studied with B3LYP quantum mechanics. This information is available free of charge via the Internet at http://pubs.acs.org.

JA048604G